

## Photodissociation of CH<sub>3</sub>CHO at 248 nm: Identification of the Channels of Roaming, Triple Fragmentation and Transition State

Yong-Chang Han,<sup>a,\*</sup> Po-Yu Tsai,<sup>b</sup> Joel M. Bowman,<sup>c</sup> and King-Chuen Lin<sup>d,\*</sup>

<sup>a</sup> *Department of Physics, Dalian University of Technology, Dalian, P. R. China*

<sup>b</sup> *Department of Chemistry, National Chung Hsing University, Taichung, Taiwan*

<sup>c</sup> *Department of Chemistry and Cherry L. Emerson Center for Scientific Computation, Emory University, Atlanta, Georgia 30322, USA*

<sup>d</sup> *Department of Chemistry, National Taiwan University, Taipei 106, and Institute of Atomic and Molecular Sciences, Academia Sinica, Taipei 106, Taiwan*

\* To whom correspondence should be addressed.

YCH: [ychan@dlut.edu.cn](mailto:ychan@dlut.edu.cn)

KCL: [kclin@ntu.edu.tw](mailto:kclin@ntu.edu.tw)

## Supporting Information

### 1. Potential Energy Surface

Previous calculations of  $\text{CH}_3\text{CHO}$  dissociation employed two PESs, which were fits to roughly 170 000 *ab initio* energies computed at the CCSD(T)/ aug-cc-pVTZ (AVTZ) level of theory and basis.<sup>1-3</sup> The dataset consists of electronic energies for complex regions and fragments of many decomposition channels. The energies of these channels were obtained by separating the fragments by about 8  $a_0$  and summing the fragment energies. We have shown that the PESs describe the open-shell complex regions like  $\text{CH}_3\cdots\text{HCO}$  and  $\text{CH}_3\text{CO}\cdots\text{H}$  realistically by interpolating through those multi-reference regions using the fragment energies.<sup>3</sup> However, comparisons of the PES against fixed one-dimensional cuts obtained directly with multi-reference MRCI(Q) calculations did show some quantitative differences,<sup>3</sup> and so we decided to supplement the existing database with additional MRCI(Q) energies. Specifically, these are obtained using the internally contracted, multireference configuration interaction (singles and doubles) method with the multireference analogue of the Davidson correction (MRCI(Q)). The orbitals of the MRCI(Q) calculations were taken from state-averaged, complete-active-space self-consistent field (SA-CASSCF) calculations. The active space used in both the CASSCF and MRCI(Q) calculations was 6 electrons in 6 orbitals. The  $S_0$ ,  $T_1$ , and  $S_1$  states were all included with equal weights in the CASSCF calculations, while the  $S_0$  and  $S_1$  states were included in the MRCI(Q) calculations. We chose MRCI(Q)/VTZ calculations for most additional energies rather than the very time-consuming MRCI(Q)/AVTZ for calculations. However, some MRCI(Q)/AVTZ calculations were done, as described below.

The procedure to add these MRCI(Q)/VTZ energies to the CCSD(T)/AVTZ data set requires care since the two methods do not produce identical absolute energies. Since our objective was to supplement the existing CCSD(T)/AVTZ database in regions of multi-reference character, we focused attention there. Also, we wanted to ensure that the previously, accurately calculated energy for  $\text{CH}_3(\text{eq}) + \text{HCO}(\text{eq})$  was

maintained. We determined the energy difference for these fragments to be 13.4 kcal/mol (with the CCSD(T)/AVTZ energy below the MRCI(Q)/VTZ one, as expected.) The difference in these energies is largely a reflection of the smaller basis used in the MRCI(Q) calculations. In addition, we examined energy differences for a number of CH<sub>3</sub>...HCO fragment configurations, using data from previous trajectories. The average difference from these configurations is 13.6 kcal/mol, which is quite close to the fragment energy difference. Therefore, we lowered all MRCI(Q)/VTZ energies, at configurations described next, by the constant amount 13.6 kcal/mol. Roughly 27 000 shifted MRCI(Q)/VTZ energies in CH<sub>3</sub>...HCO and CH<sub>3</sub>CO...H regions were added to the previous dataset for a new global fit. The configurations were obtained from numerous trajectories run on the previous PES in the regions of CH<sub>3</sub>...HCO configurations where the carbon-carbon bond distances varied from 4 to 9 a<sub>0</sub> and also for many CH<sub>3</sub>CO...H configurations. For the multi-reference biradical (CH<sub>2</sub>CH<sub>2</sub>O) region between acetaldehyde and oxirane, roughly 3000 energies were calculated with MRCI(Q)/AVTZ theory and basis with a (6, 6) active space, and were shifted by 7.90 kcal/mol (the average energy difference between the MRCI(Q)/AVTZ and CCSD(T)/AVTZ calculations) before being added to the large CCSD(T)/AVTZ data base. In addition, we performed CCSD(T)/AVTZ calculations of roughly 5000 energies in the vinyl alcohol and hydroxyethylidene regions.

All the energies, new and previous ones, were obtained with the MOLPRO suite of electronic structure program.<sup>4</sup> Currently, the entire dataset of roughly 200 000 energies was fit, as before, using a basis of permutationally invariant polynomials in Morse-like variables in all the inter-nuclear distances.<sup>5</sup> This choice of basis leads to the important property of invariant with respect to all permutations of like nuclei. The fit is of maximum fifth order and has an RMS fitting error of 2.9 kcal/mol, for energies up to 160 kcal/mol above the CH<sub>3</sub>CHO minimum.

Here we give in Table S1 a comparison of energies from the current PES with CCSD(T)/CBS+CV benchmark calculations.<sup>2</sup> For the indicated stationary points numbered 1-11, the present PES has the same accuracy as the earlier PES.<sup>2</sup> For the stationary points numbered 12-21, the present PES has improved accuracy compared

to the earlier PES, with the average error of these stationary points lowered from 6.9 to 2.3 kcal/mol. In addition, the regions related to the complexes of  $\text{CH}_3\cdots\text{HCO}$  and  $\text{CH}_3\text{CO}\cdots\text{H}$  have also been improved. Also note that the threshold for formation of  $\text{CH}_3\text{CO}+\text{H}$  is more accurate on the new PES compared to the previous one, which is roughly 4 kcal/mol higher.

Finally, we show in Figure S1 selected cuts from the global minimum to the  $\text{CH}_3+\text{HCO}$  and  $\text{H}+\text{CH}_3\text{CO}$  fragments from the PES and from MRCI(Q)/VTZ calculations. These energies are all relative to the acetaldehyde global minimum. These potential cuts pass through the regions of multi-reference character, and as seen the current PES is in good accord with the direct MRCI(Q)/VTZ energies.

**Table S1.** Comparison of the potential energy surface (PES) and the *ab initio* benchmark electronic energy calculations (without ZPE) for selected stationary points.<sup>a</sup> The energies are relative to the acetaldehyde global minimum in kcal/mol.

	CCSD(T)/CBS+CV	PES
1. acetaldehyde	0.0	0.0
2. vinyl alcohol	9.1	12.5
3. hydroxyethylidene	50.8	53.6
4. CH <sub>4</sub> +CO	-2.0	-1.1
5. CH <sub>2</sub> CO+H <sub>2</sub>	35.2	40.7
6. CH <sub>3</sub> +HCO	90.8	91.5
7. CH <sub>3</sub> CO+H	95.6	96.3
8. CH <sub>2</sub> CHO+H	102.5	104.6
9. CH <sub>3</sub> +CO+H	110.5	111.9
10. TS4(1-4)	87.5	89.0
11. TS5(1-5)	86.0	92.1
12. TS1 (1-2)	70.8	72.3
13. TS2 (2-3)	75.5	78.3
14. TS3 (1-3)	83.0	84.5
15. oxirane	29.2	29.3
16. IM (CHCH <sub>2</sub> OH)	96.4	93.0
17. H <sub>2</sub> CC+H <sub>2</sub> O	86.9	88.9
18. C <sub>2</sub> H <sub>2</sub> +H <sub>2</sub> O	42.1	47.9
19. TS6 (2-17)	94.7	95.6
20. TS7 (2-18)	96.7	93.5
21. TS8 (1-15)	85.0	86.5

<sup>a</sup>The notation TS*k*(*n-m*) refers to the TS between species *n* and *m* and *k* is an ordering label.

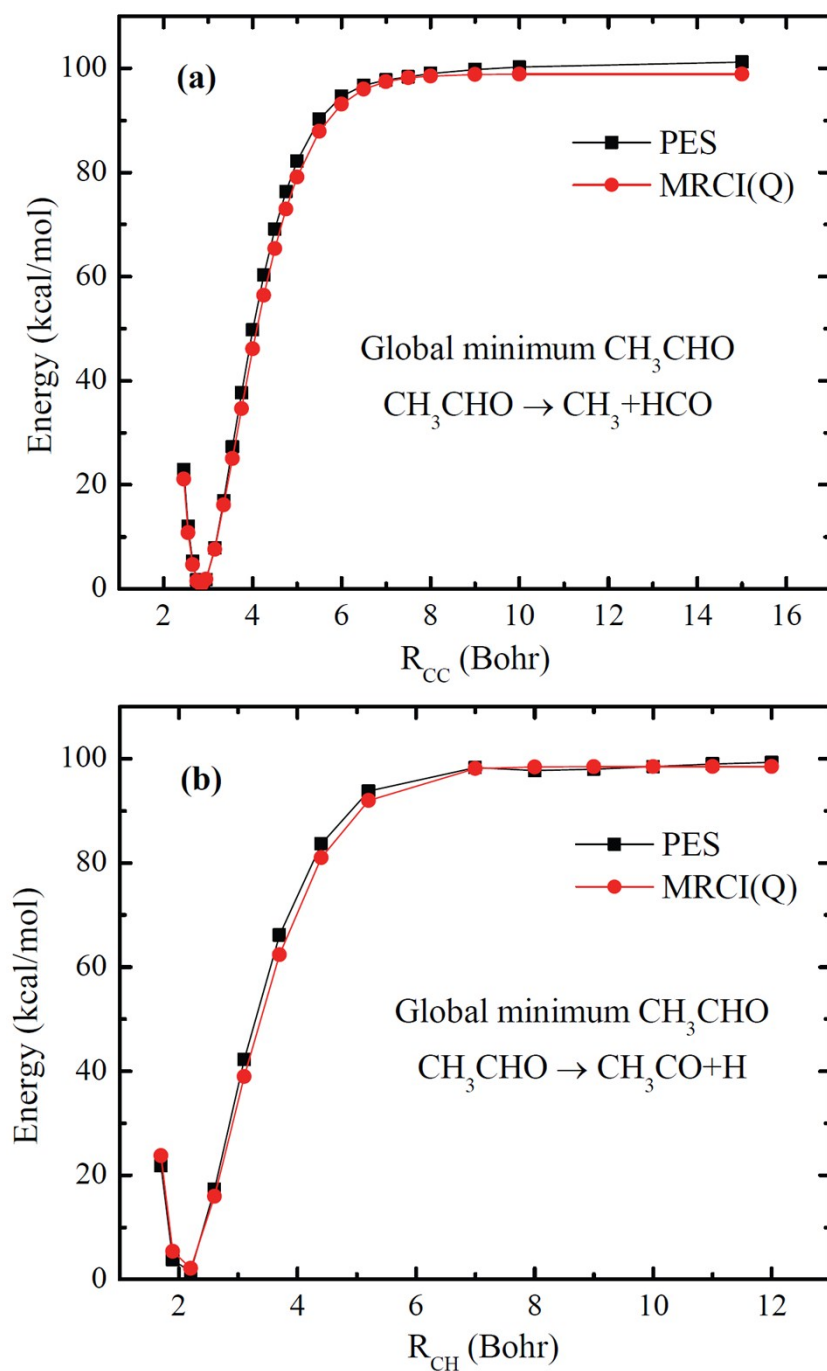


**Fig.S1** Potential cuts from the acetaldehyde global minimum to the indicated radical products from the PES and direct MRCI(Q)/AVTZ calculations. The energies are relative to the acetaldehyde global minimum.

## 2. Analysis of CH<sub>4</sub> vibrational energy distribution

The method used to estimate vibrational population distribution of CH<sub>4</sub> is similar to a prior study.<sup>6</sup> The CH<sub>4</sub> vibrational distribution is extracted from its infrared emission spectrum around 2550~3100 cm<sup>-1</sup>, which is assigned as CH<sub>4</sub>  $\Delta v_3 = -1$  emission. The pure vibrational spectrum of CH<sub>4</sub> is then deconvoluted by taking into account rotational profile via the built-in function of non-negative least-squares fit in MATLAB. The pure vibrational spectrum is obtained as discrete data points with 6 cm<sup>-1</sup> interval, as shown in Figure S2. Given the rotational constants,<sup>7</sup> the rotational profiles are characterized with temperature assumed at 500 K. The procedure to obtain vibrational population distribution of CH<sub>4</sub> from the infrared emission spectrum is then described as follows.

(1) Line position calculations: There are four normal modes in CH<sub>4</sub> molecule, one non-degenerate stretching mode ( $v_1$ ), one doubly-degenerate bending mode ( $v_2$ ) and three triply-degenerate modes ( $v_3$  and  $v_4$ ). The doubly degenerate mode contains an extra vibrational angular momentum quantum number  $l$  with the degeneracy determined by possible values of  $l$  ( $l = -v, -(v-2), \dots, v-2, v$ ), while each triply-degenerate mode consists of two angular momentum quantum numbers ( $l$  and  $kl$ ,  $kl = l, l-1, \dots, -l$ ). The possible value of  $l$  in triply degenerate mode is positive ( $l = v, v-2, \dots, 1$  or  $0$ ), with the degeneracy  $(2l+1)$  in each  $|v, l\rangle$  sublevel. All the possible infrared active states and the corresponding line positions which can contribute emission spectrum are calculated via analytical equation of anharmonic vibrational energy.<sup>8</sup> The vibrational states are labeled as  $(v_1, v_2, l_2, v_3, l_3, v_4, l_4)$ . The harmonic and anharmonic coefficients which were used in calculations of line position are  $\omega_i$ ,  $X_{ij}$ , and  $G_{ij}$  coefficients as listed in table III of ref.9.

(2) Number of states and the allowed transitions: both the number of states and allowed transitions increase with increasing the energy and these two factors compensate for each other when counting the vibrational population. If one considers only the increment of state number, then the vibrational population at higher energy states is overestimated, but underestimated at lower energy. For each  $|v_3, l_3\rangle$  sublevel,

the number of allowed transitions to lower  $|v_3-1, l_3'\rangle$  sublevels are determined by considering (a) the angular momentum conservation of one-photon emission process ( $|\Delta l| \leq 1$ ) and (b) infrared-allowed irreducible representation (symmetry species  $T_2$  in point group  $T_d$ ) derived from direct product of initial-final states ( $v_3, l_3, kl_3 \rightarrow v_3-1, l_3', kl_3'$ ). The representations of symmetry operator in  $T_d$  point group for  $|l, kl\rangle$  sublevels are given in ref.10. The direct product of upper and lower  $|l, kl\rangle$  sublevels is reduced to sum of irreducible representations and transitions that contain those  $T_2$  species give contribution to infrared emission intensity. Note that not every initial  $kl$  sublevels has the same number of transition to final sublevels. For the same  $|v, l\rangle$ , it will be treated as equally populated at different  $kl$  sublevels in later step of analysis. It is convenient to consider the average number of transition in  $|v_3, l_3, kl_3\rangle$  sublevel by number of initial  $|v_3, l_3, kl_3\rangle$  sublevel.

(3) Line intensity calculations: Einstein spontaneous emission coefficients are estimated in terms of standard IR harmonic line-strength factors of pure vibrational transition. The validity of harmonic line-strength factors in current case has been examined in ref.6.

(4) Maximum entropy model fit: Given the line positions and Einstein spontaneous emission coefficients calculated, the vibrational distribution may be extracted from the pure vibrational spectrum with the aid of maximum entropy assumption. Note that all the levels which contribute to the infrared emission spectrum within the same binned interval are equally populated.



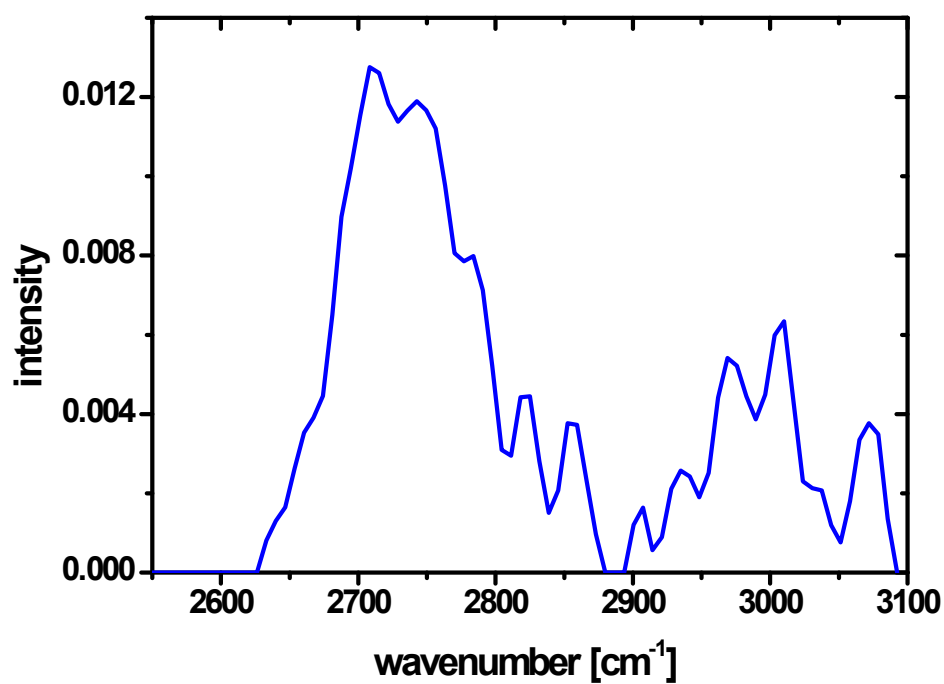


**Figure S2** The pure vibrational spectrum (binned at 6  $\text{cm}^{-1}$  interval) after deconvoluting rotational profile from  $\text{CH}_4$  time-resolved infrared emission spectrum at 5  $\mu\text{s}$  delay.

## References

- [1] B. R. Heazlewood, M. J. T. Jordan, S. H. Kable, T. M. Selby, D. L. Osborn, B. C. Shepler, B. J. Braams, and J. M. Bowman, *Proc. Natl. Acad. Sci. U.S.A.* 2008, **105**, 12719-12724.
- [2] B. C. Shepler, B. J. Braams, and J. M. Bowman, *J. Phys. Chem. A* 2008, **112**, 9344-9351.
- [3] B. C. Shepler, B. J. Braams, and J. M. Bowman, *J. Phys. Chem. A* 2007, **111**, 8282-8285.
- [4] MOLPRO, a package of *ab initio* programs written by H.-J. Werner, P. J. Knowles, R. Lindh *et al.*, see <http://www.molpro.net>.
- [5] B. J. Braams and J. M. Bowman, *Int. Rev. Phys. Chem.* 2009, **28**, 577-606.
- [6] B. R. Heazlewood, M. J. T. Jordan, S. H. Kable, T. M. Selby, D. L. Osborn, B. C. Shepler, B. J. Braams, and J. M. Bowman, *Proc. Nat. Acad. Sci. USA* 2008, **105**, 12719-12724.
- [7] D. L. Gray and A. G. Robiette, *Mol. Phys.* 1979, **37**, 1901-1920.
- [8] G. Herzberg, *Infrared and Raman Spectra of polyatomic molecules, molecular spectra and molecular structure*, Van Nostrand, 1945
- [9] T. J. Lee, J. M. L. Martin, and P. R. Taylor, *J. Chem. Phys.* 1995, **102**, 254-261.
- [10] H. A. Jahn, *Proc. R. Soc. Lond. A* 1938, **168**, 469-495.